Coherent thermodynamic model for ice I h -A model case for complex behavior

Wilfried Holzapfel, Stefan Klotz

Coherent thermodynamic model for Ice Ih - A model case for complex behavior

Wilfried B. Holzapfel[1, a)] and Stefan Klotz[2]

[1)]*Department Physik, Universität Paderborn, D-33095, Germany*

[2)]*IMPMC, CNRS UMR 7590, Sorbonne Université, 4 Place Jussieu, F-75252 Paris,*
France

(Dated: 5 October 2021)

New data on the variation of the thermal expansion of ice Ih with temperature at
ambient pressure together with new evaluations of the bulk modulus and earlier data
for the heat capacity provide the basis for a coherent thermodynamic modeling of the
main thermo-physical properties of ice Ih over its whole range of stability. The quasi-
harmonic approximation with one Debye and 7 Einstein terms, together with explicit
anharmonicity, represents the dominant contributions next to minor "anomalies"
from hydrogen ordering and lattice defects. The model fits accurately the main
features of all experimental data and provides a basis for the comparison with earlier
determinations of the phonon density of states and the Grüneisen parameters.

[a)]Corresponding authors: holzapfel@physik.upb.de, Stefan.Klotz@upmc.fr

I. INTRODUCTION

Ice Ih can be considered as a prototype of solids with anomalous thermo-physical properties not only due to the negative slope of its melting curve[1–3] and its negative thermal expansion at low temperature[4–6] but also due to its anomalous specific heat capacity[7–11] showing a slow linear increase over a wide range in temperature (at ambient pressure) and a correspondingly strong variation of its thermal Debye temperature[8], related to a very wide and strongly structured phonon density of states (PDOS)[12–15]. Various first-principles calculations of thermophysical properties of ice Ih[16–19] have provided a solid background for a better understanding of both the approximations involved in theses calculations and for the basic physics of ice. However the results do not represent the thermophysical properties within the accuracy of the experimental data. Also, the two purely empirical description of the thermodynamics of ice Ih by different series expansions[2,3] do not represent the thermophysical properties within the accuracy of the experimental data. In the first case[2], the negative thermal expansion at low temperature was obviously considered as an experimental artifact and replaced by a positive interpolation down to low temperatures. In the other case[3], the series expansion was restricted to temperatures above 180 K. On the other hand, the properties of ice Ih in wide ranges of pressure and temperature are of basic interest to glaciologists as well as for models of icy planets and moons. To the best of our knowledge no comprehensive thermodynamic model for the thermo-physical properties of ice Ih has been reported so far representing all the presently available experimental data within their given accuracy and providing the basis for the prediction of all theses properties over the entire range of existent of ice Ih.

The present study was motivated by the observation that although the use of two Debye and one Einstein term provided a very good description of the recent thermal expansion data[6], these three terms are completely insufficient for the representation of the heat capacity: It needs a better description of the PDOS by at least one Debye term and more than 2 Einstein terms, whereby the PDOS derived from the neutron scattering data[12–15] provide good guides for the selection of the representative Einstein temperatures.

The present approach is intended to model the dominant thermo-physical properties of ice Ih. At the same time it helps for the evaluation of the smaller, but significant other contributions detected first in the heat capacity[10]. These were attributed to a "proton glass

(PG) transition"[10] and are clearly visible in more recent volume expansion data[5] where it was interpreted as arising from solitons, i.e. localized librational movements of H_2O molecules. Further anomalies were attributed to ferroelectric ordering, to the ice Ih-XI phase transition and to special relaxation effects at low temperatures[20,21].

II. THE MODEL

Coherent thermodynamic models for all thermo-physical properties of solids are usually based on the formulation of the partition function which provides, being a fundamental function of the system, the Helmholtz free energy $F(T, V, n, ...)$[22,23] as a function of temperature T, volume V, particle number n, and often other parameters which we do not need in the present case. If we keep the particle number fixed to 1 mole, the state of the system is characterized just by the two state variables T and V, whereby V as well as all the other extensive functions, like the free energy $F(T, V)$, the internal energy $U(T, V)$, and the entropy $S(T, V)$, are represented in the following as molar quantities. The free energy $F(T, V)$ includes two parts, the energy of the ground state (or "cold part") $E_{zT}(V)$, and thermal contributions $F_{th}(T, V)$:

$$F(T, V) = E_{zT} + F_{th}(T, V) \tag{1}$$

For convenience we include the zero-point energy of the phonons in the ground state energy $E_{zT}(V)$. Correspondingly, the pressure P and the bulk modulus K are also separated in two parts::

$$P(T, V) = \partial F(T, V)/\partial V = P_{zT} + P_{th}(T, V) \tag{2}$$

$$K(T, V) = -V \partial P/\partial V = K_{zT}(V) + K_{th}(T, V) \tag{3}$$

For the limited stability range of ice Ih, the ground-state energy and the corresponding pressure and bulk modulus at zero temperature are well represented by the Murnaghan forms[24]:

$$E_{zT}(V) = \frac{V K_0}{K_0'(K_0' - 1)} \left[(\frac{V_0}{V})^{K_0'} + K_0' - 1 \right] \tag{4}$$

3

$$P_{zT}(V) = \frac{K_0}{K_0'}\left[(\frac{V_0}{V})^{K_0'} - 1\right] \tag{5}$$

$$K_{zT}(V) = K_0(\frac{V_0}{V})^{K_0'} \tag{6}$$

Thereby V_0 stands for the volume, K_0 for the bulk modulus and K_0' for its pressure derivative at zero temperature and ambient pressure.

The dominant part of the thermal free energy $F_{th}(T,V)$ and of the thermal pressure $P_{th}(T,V)$ of insulators comes from phonons and is usually described in the quasi-harmonic phonon approximation as an integral or a sum over contributions from Einstein-oscillators, whereby the volume-dependent frequencies $\nu(V)$ of the oscillators are commonly replaced by corresponding Einstein-temperatures $\theta(V) = h\nu(V)/k_B$. The free energy of one Einstein term (without its zero-point energy) is

$$f_E(T,\theta) = k_B T \; ln(1 - exp(-\theta/T)) \tag{7}$$

whereby we use lower case letters for all the functions related to single modes in contrast to capital letters used for molar quantities. The corresponding formulas for the internal energy $u_E(T,\theta)$, heat capacity $c_E(T,\theta)$, thermal pressure $p_E(T,\theta)$ and thermal contribution to the bulk modulus $k_E(T,\theta)$ are given in the Appendix.

Convenient relations for the volume dependence of the Einstein temperature θ, its first-order Grüneisen parameter γ and its second-order Grüneisen parameter Γ are provide by the form:

$$\theta_{qh}(V) = \theta \cdot (V/V_0)^{\gamma(\Gamma-1)} exp\left[\gamma\Gamma \cdot (1 - (V/V_0))\right] \tag{8}$$

which gives

$$\gamma_{qh}(V) = -\partial ln(\theta_{qh}(V))/\partial ln(V) = \gamma\left[1 - \Gamma \cdot (V/V_0)\right] \tag{9}$$

$$\Gamma_{qh}(V) = \partial ln(\gamma_{qh}(V))/\partial ln(V) = \Gamma V/\left[V_0 - \Gamma \cdot (V - V_0)\right] \tag{10}$$

with the ambient pressure $(V = V_0)$ values θ, γ and Γ. For simple, monatomic, nonmetallic, crystalline materials, the Debye model[25] provides a good approximation for the phonon density of state $(PDOS)$ in the form:

4

$$PDOS_D(T, \theta_D) = 3N \ T^2/\theta_D^3 \tag{11}$$

for N oscillators and a cutoff at the volume dependent Debye temperature θ_D. The quasi-harmonic thermal free energy in this Debye model has then the form:

$$F_D(T, \theta_D) = \int_0^{\theta_D} PDOS_D(\tau, \theta_D) f_E(T, \tau) d\tau \tag{12}$$

and the corresponding Debye free energy $f_D(T, \theta_D)$, internal energy $u_D(T, \theta_D)$ and heat capacity $c_D(T, \theta_D)$ per mode are given in the Appendix.

In the more general case of crystalline solids with more than one atom per unit cell the Debye approximation remains reasonable for the low energy acoustic phonons, and the remaining phonon contributions are usually well represented by a few "representative" Einstein terms. In this way one obtains for the quasi-harmonic contribution to the molar free energy:

$$F_{qh}(T, V) = N \sum_i^n w_i f_i(T, V) \tag{13}$$

with N for the number of molecules per mole and the weights w_i for the free energies per mode $f_i(T, V)$, whereby the index i refers to the fact that each term with its volume dependence includes the parameters θ_i, γ_i, and Γ_i. In addition, the index i=0 refers to the Debye form (A5) and $i >0$ to the Einstein form (7). In the same way one obtains the other quasi-harmonic contributions to internal energy, heat capacity, total pressure and bulk modulus as weighted sums over the individual terms.

The question is now, how many Einstein terms are needed to represent the experimental data within their given accuracy? Information on the phonon spectrum for ice Ih from the neutron scattering function[14] motivated Fortes[6] to evaluate his thermal expansion data at ambient pressure with two Debye and one Einstein term. If we use the form (A3) for the contribution of a single Debye or Einstein term to the thermal pressure together with the inverted form (5) for the thermal expansion at ambient pressure as a function of the thermal pressure together with the assumption that the thermal pressure is very small with respect to the bulk modulus and the volume dependence on the right hand side can be neglected, we get as a good first order approximation:

TABLE I. Best fitted parameters for Debye or Einstein temperatures θ_i and Grüneisen parameters γ_i together with normalized standard deviations σ for the representation of the thermal expansion data of Fortes[6] with various combinations of Debye, pseudo-Debye and Einstein terms labeled with D, PD and E for the terms used in the form (14).

Model	$\theta_1(K)$	$\theta_2(K)$	$\theta_3(K)$	γ_1	γ_2	γ_3	σ
Fortes	87	513	1254	-0.70	1.32	1.33	1.00
2D1E	87	513	1254	-0.69	1.32	1.33	0.90
2PD1E	86	513	1239	-0.69	1.32	1.28	0.90
1PD2E	65	376	1079	-0.43	1.18	1.59	1.08
0PD3E	41	376	1211	-0.40	1.16	1.37	1.00

$$V_{qh}(T) = V_0 \left(1 + \frac{N K_0}{V_0} \sum_{i}^{n} \gamma_i w_i u_i(T, \theta_i) \right) \tag{14}$$

If one would assume that the two transverse and one longitudinal acoustic branches are represented by the two Debye terms and the three degrees of freedom for the librational modes by one Einstein term, the corresponding weights 2:1:3 in the quasi-harmonic approximation result in a very poor description of the heat capacity. If one tries to fit the data for the heat capacity[7,8,10,11] with theses three terms one gets the weights 0.78, 3.10 and 4.23, but still with large systematic deviations indicating that one needs a model with more Einstein terms. However, for the following discussion of different forms for the thermal expansion we may just use these weights to represent the corresponding Grüneisen parameters γ_i with the use of the values from Ref.[6] V_0=19.304 cm^3/g and K_0=10.713 GPa in the form (14). In the first line of Table I we reproduce just the corresponding data of Fortes' original fit[6], whereby we present only the decimals needed for this comparison. The corresponding residues of the thermal expansion data of Fortes[6] from his fitted form are illustrated in fig. 1 together with the deviations of the other optimized forms from his original relation.

For comparison, we have refitted the parameters of the form (14) with the algorithm of Mathcad, which we used for all the present calculations, and noticed only a small decrease in the standard deviation σ (second row in Table I marked 2D1E) probably due to a different weighting scheme. The blue dash-dotted line in fig. 1 illustrates the very small difference of
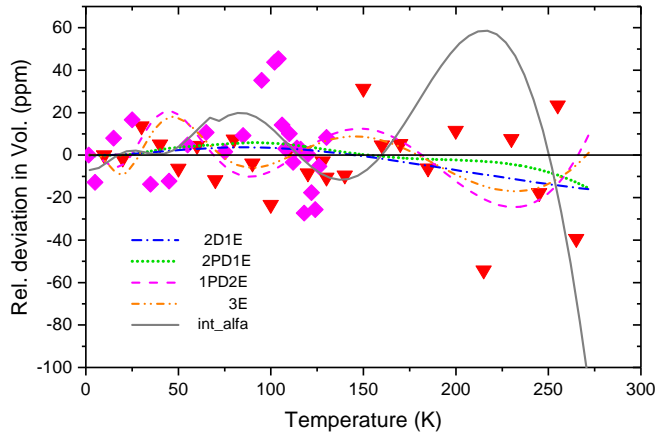
FIG. 1. Relative deviations of the volume data of Fortes[6] in ppm (red and pink diamonds) with respect to his best fit with 2 Debye and 1 Einstein term as black base line. Additional curves show the small deviations of the present refit with 2 Debye terms and 1 Einstein term as blue dash-dotted line and the fits with 2 pseudo-Debye and 1 Einstein term (green dotted curve), with 1 pseudo-Debye and 2 Einstein terms (dashed pink curve) and with 3 Einstein terms only (orange dash-double-dotted curve), respectively. Integration of Fortes' analytic form for the thermal expansivity (grey solid curve, "int-alfa") shows significantly larger deviations.

this fit. Since the original Debye function with their integral form considerably slows down all least square fits, we applied the simpler pseudo-Debye form[26–29]. All the refinements were performed with the pseudo-Debye function given in the Appendix.

We tested the pseudo-Debye form with a fit of the form (14) to the experimental data (third row in Table I marked 2PD1E and green dotted line in fig. 1) and obtained almost the same results in comparison with the previous fit, justifying the use of this more efficient form in all the following calculations. The form with one pseudo-Debye term and two Einstein terms (row 4 in Table I and thin pink dashed line in fig. 1) deteriorated very slightly the fit but provides still the expected T^4-variation at low temperatures in contrast to the fit with three Einstein terms (row 5 in Table I and thin dashed-double-dotted curve in fig. 1). This would be the simplest form for the representation of the thermal expansion coefficient, still with much smaller systematic deviations from the data than the previously proposed

7

form[6]. The deviation in the thermal expansion calculated by integration of Fortes' previous form is shown in fig. 1 as the grey line. One may notice that the Debye temperatures in the first and second column of Table I are significantly larger than the corresponding Einstein temperatures due to the fact that the Einstein temperatures correspond to the centers of gravity of the respective Debye spectrum.

Before we evaluate in detail all the available data for the volume expansion[4–6] the question remains, how many Einstein terms do we need, to represent the heat capacity at ambient pressure within the limits of the experimental accuracy.

III. HEAT CAPACITY AT AMBIENT PRESSURE

In the fit of the experimental C_v-data[7–11] we use only the more accurate data sets[7,10,11] and start with constraining the Debye term with respect to the data at the lowest temperatures[11] as illustrated in the double logarithmic plot of fig. 2.
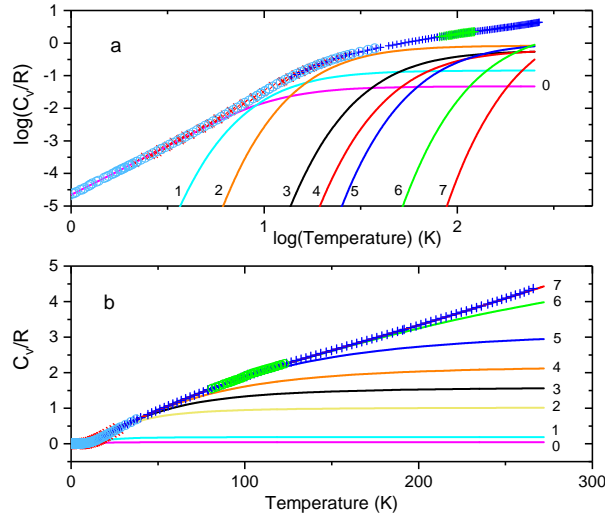
FIG. 2. a) Contributions of the Debye term $(i = 0)$ and the 7 Einstein terms to the heat capacity (in units of R) at ambient pressure in log-log scale versus temperature and b) Sum of the contributions to the heat capacity on linear scales. Symbols are experimental data from refs.[7,10,11]

By trial and error, the plots in fig. 2 provided good starting values for the refinement of 1 Debye and 7 Einstein terms with the results for the Debye temperature θ_0 and the seven Einstein temperatures θ_i as well as for their weights w_i given later in Table II together with the other parameters for this 1D7E-model. Thereby, a compromise had to be found in the

8
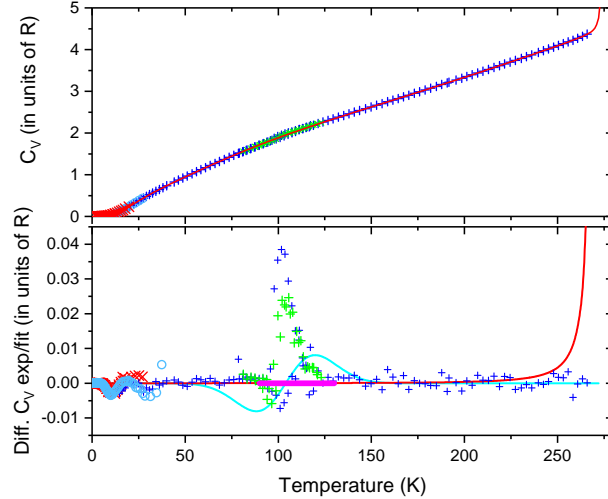
FIG. 3. Experimental heat capacity data[7,10,11] (upper) and deviation from the fitted relation for C_v (lower) including contributions from the PG-transition (light blue) and explicit premelting anharmonicity (red). The anomalous region (thick pink) has been excluded in the fit.

number of terms, because a larger number of terms improves the quality of the fit but leads to physically unreasonable parameters like negative weight and large uncertainties due to stronger correlations.

Fig. 2 illustrates that the C_v-data deviate already at temperatures below 10 K from the normal Debye behavior and the weight of the Debye term given in Table II is though very small. The almost linear increase of C_v over a wide range in temperature and the large number of Einstein terms indicate here again that the PDOS must deviate strongly from a simple Debye form. The quality of the fit is illustrated in fig. 3 by the residues with respect to the quasi-harmonic contribution, whereby we excluded in the fit all the data in the region of anomalous behavior around 100 K, the region marked in pink in fig. 3.

This anomaly around 100 K had been attributed to molecular disorder[10] and was studied in more detail recently by thermal dilatometry[5] and neutron scattering[6]. It should be noted that the original term "proton glass"[10] is misleading since the molecules are still intact. What is presumably meant is a glass behaviour in the molecular dipole orientations as the reorientation dynamics becomes extremely slow at these temperatures. It is visible in fig. 3 as a strong peak with significant scattering of the data. Since no theory exists from which an analytical expression for the associated heat capacity could be derived, we simply describe

it empirically by:

$$C_{PG}(T) = R \ \frac{2w_{C_{PG}}}{\Delta T_{C_{PG}}} \left(\frac{T - T_{C_{PG}}}{\Delta T_{C_{PG}}}\right) exp\left(-\left(\frac{T - T_{C_{PG}}}{\Delta T_{C_{PG}}}\right)^2\right) \qquad (15)$$

with the parameters $w_{C_{PG}} = 0.214$, $T_{C_{PG}} = 104$ K and $\Delta T_{C_{PG}} = 22$ K and represented in fig. 3 by the light blue line. Since large hysteresis and dependence on heating rate was observed for this transition[10] as illustrated by the green and blue crosses for the two different runs, we have excluded the range marked by the pink solid line in this fit. This transition may be related also to the disorder in the structure of ice Ih observed at first as an anomaly in the entropy[30] and studied in more detail in recent years[16,18,31–34]. The corresponding disorder entropy is not included in the present quasi-harmonic approach, but could be added easily later, and it is not clear whether there are other contributions from the disorder to the heat capacity which are included here in the quasi-harmonic terms.

Slightly before melting a small additional contribution shows up as "premelting anharmonicity" (thin red line) related also to the occurrence of defects[35,36], which we model by:

$$C_a(T, T_a) = w_a \ R \ T_a T(T_a - T)^{-2} \qquad (16)$$

with the corresponding free energy

$$F_a(T, T_a) = w_a \ R \ ln(1 - \frac{T}{T_a}) \qquad (17)$$

and the internal energy

$$U_a(T, T_a) = w_a \ R \ T_a \left(\frac{T}{T_a - T} + ln(1 - \frac{T}{T_a})\right) \qquad (18)$$

with weight $w_a = 8.0 \cdot 10^{-5}$ and $T_a = 280$ K.

Some problems with the quasi-harmonic approximation are noticed when one uses the experimental data[10,11] to calculate the corresponding calorimetric Debye temperature $\theta_C(T)$[8,38] shown in fig. 4. At first one can notice a significant decrease of $\theta_C(T)$ at low temperatures (T $<$ 10 K), up to about 13 K, which can be attributed to a deviation of the PDOS from Debye type T^2-behavior already at theses low energies represented by the first Einstein term in the present model. A stronger Debye contribution would have resulted in a horizontal start at low temperatures. There appears to be a horizontal part below 5 K, however it does not fit to the expected low energy limit determined as acoustic Debye temperature θ_A from
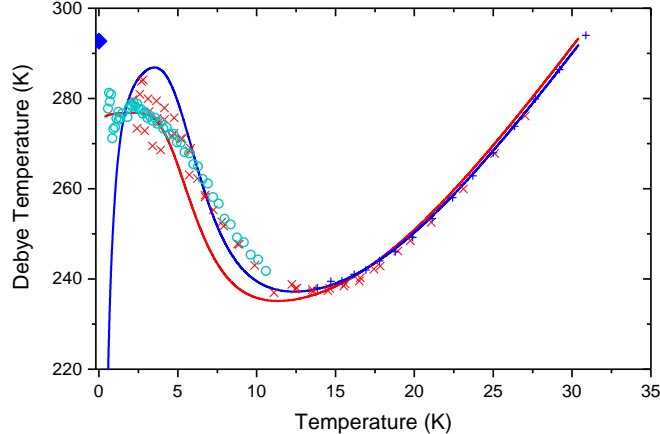
FIG. 4. Comparison of the acoustic θ_A (blue diamond)[37] and the calorimetric Debye temperature θ_C (circles and crosses) below 30 K with the present quasi-harmonic curve (red line) and a rough fit (blue line) illustrating possible quantum glass contributions.

ultrasonic measurements of the elastic coefficients[37]. This difference may be typical for the quantum effects in glasses at low temperatures[39] which lead to a linear contribution to the heat capacity in the milli-Kelvin region but would not effect the acoustic Debye temperature. From this point of view it would be interesting to perform a detailed study of the heat capacity in this very low temperature region, which would than allow to refine the present model further for this region. Due to the strong weight of the many data points below 5 K the fitted curve represents these data very well but deviates significantly in the region around 10 K. This deviation could be modeled by an additional Einstein term. However as long as we have no quantitative information on the possible quantum glass contribution this rather small difference (in absolute values) will be considered as an uncertainty of the present model.

IV. THERMAL EXPANSION AT AMBIENT PRESSURE

In the next step we want to find good starting values for the first-order Grüneisen parameters γ_i (Table II) for the present 1D7E-model with its single Debye and 7 Einstein terms from fits of the form (14) to various data of the thermal volume expansion.

11
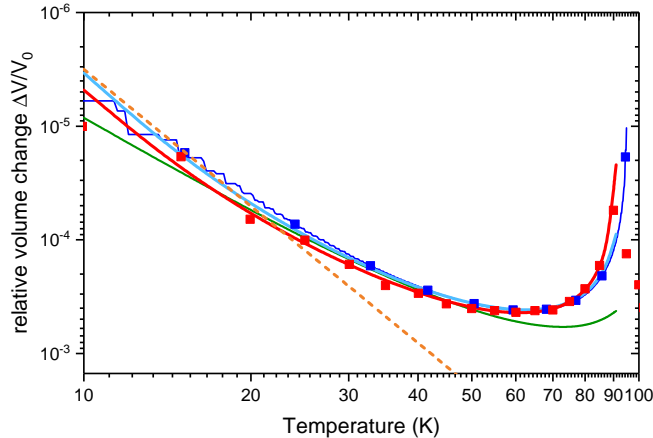
FIG. 5. **Relative** volume change in the low temperature region on double logarithmic scale. The dilatometry data[5] are represented by the blue stepped curve with the blue squares as smoothed values, and the solid light blue curve corresponding to the present best 1PD7E-fit. The green curve reproduces the original best fit of earlier diffraction data[4] and the red squares together with their best 1PD7E-fit (red curve) illustrate the later diffraction data[6]. The dashed orange line stands for the expected T^4-behavior at low temperature.

Although the dilatometry data have a much higher precision than the diffraction data at low temperatures, they needed a 6 ppm decrease in the absolute values to match the diffraction data at 0 K. The differences over the full range in temperature are shown in fig. 6.

One may notice that the deviation of the dilatometry data from the later diffraction data is only 6 ppm below 50 K where the diffraction data provide a better reference for V_0. More significant are the differences at higher temperatures (fig. 6). The dilatometry data show some small wiggles which represent additional deviations from the 1PD7E-model, though in the diffraction data[6] similar wiggles are not observed or resolved. In addition, the large difference between the dilatometry and the diffraction data in the upper temperature range needs some special attention.

On should recall that the dilatometric method probes macroscopic properties (changes in the length along crystallographic axes and hence the volume of the sample), whereas the diffraction technique provides microscopic information on the crystal structure and the
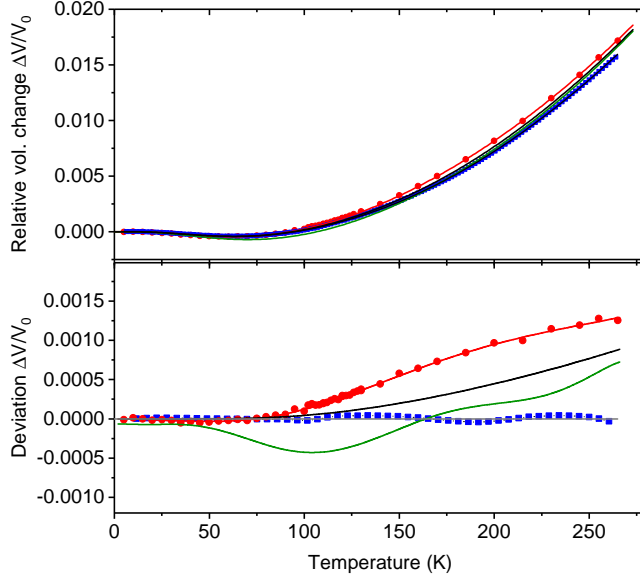
FIG. 6. Relative volume change (upper) and deviation (lower) from the dilatometry data[5] (blue squares with the blue line being a 1PD7E fit). X-ray diffraction data[4] are represented by the green curve and neutron diffraction results[6] by the red dots and the red curve being the corresponding 1PD7E fit. The black curve represents an estimated average used in this work as reference data.

corresponding unit cell. Differences at elevated temperature have been attributed in many cases to the thermal excitation of defects. A difference of 1% just before melting seems not to be too large. However, in general, defects are expected to increase the volume[35,36]. Maybe this is an other anomaly of ice Ih.

With all these uncertainties we use just a reasonable average curve as reference for our model as indicated by the black curve in fig. 6. This reference fits perfectly the dilatometry data in the lower temperature range and gives a reasonable average at higher temperatures. It corresponds to the 1PD7E-form with just a small change in γ_5 given in Table II. The corresponding parameters for the preliminary description of the experimental data by theses refinements are presented in Table II as "Our ref.".

One may notice in Table II that the largest differences in the γ_j occur for the first Debye term and the last Einstein term. This reflects the fact that, on the one hand, significant differences in the thermal expansion data are observed at very low temperature (fig. 5, giving the variation at low temperatures on double logarithmic scale) and, on the other hand, in the upper temperature range (figure 6, presenting the differences with respect to the best

13

TABLE II. Preliminary parameter values for the present 1PD7E-model from independent fits of the data to the heat capacity, thermal expansion and bulk modulus at ambient pressure. $\gamma_{a,i}$, $\gamma_{b,i}$, and $\gamma_{c,i}$ correspond to fits to data from refs.[4],[6], and[5], respectively. "Our ref." refers to the parameter set based on the black line in fig. 6.

	0	1	2	3	4	5	6	7
$\theta_i(K)$	55	55	104	227	324	435	955	1693
w_i	0.044	0.142	0.844	0.566	0.626	1.041	2.596	5.94
$\gamma_{a,i}$	-0.71	-1.91	-0.56	0.72	2.51	2.11	0.63	1.12
$\gamma_{b,i}$	-1.41	-1.78	-0.25	0.94	2.22	1.77	0.76	0.65
$\gamma_{c,i}$	-0.61	-1.52	-0.34	0.94	1.94	1.35	1.41	0.09
$Our\ ref.$	-0.61	-1.52	-0.34	0.94	1.94	1.54	1.41	0.09
Γ_i	-18.5	-18.5	-92.9	3.80	8.49	-8.25	-0.93	-0.93

fit of eq. 14 to the dilatometry data[5]). The less negative values of γ_0 in this case fit also better to the mostly positive pressure dependencies of the elastic coefficients C_{ij}[40,41] and to the dispersion of the mode-Grüneisen parameters measured by neutron scattering under pressure[15].

V.   BULK MODULUS AT AMBIENT PRESSURE

When one compares the data for the temperature dependence of the bulk modulus at ambient pressure[2,6,42,43] in fig. 7, one can notice at first that there is a reasonable agreement in the middle of the given temperature range. In the upper temperature range the differences remain small compared with the uncertainty of the data. However, at low temperatures the differences are more significant. The evaluations[2,6] were primarily based on a complete set of elastic constants determined by ultrasonic measurements[42] covering the range from 60 K to 110 K, various data at fixed temperatures in the range 240-260 K[40,44–46] and suitable interpolation schemes between. From this point of view extrapolations[2,6] to temperatures below 60 K are not based on experimental data. The most recent study[43], on the other hand, covers the range from 50 K to 273 K and takes into account all the earlier measurements. Therefore we give this evaluation twice as much weight when we fit all the data together

with our 1PD7E-model.
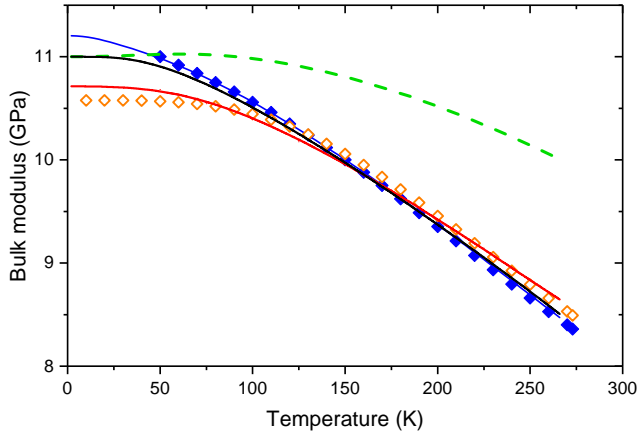
FIG. 7. Comparison of various reference data for the temperature dependence of the bulk modulus at ambient pressure. The reference data from 2006[2] are represented by orange open diamonds. A later evaluation[6] based on published low-temperature ultrasonic data and Brillouin results at higher temperatures is shown as red line. The most recent evaluation[43] is marked by the blue line with the blue diamonds. Our best fit, discussed in the text, is represented by the black line. The green dashed line illustrates the cold lattice contribution.

Our best fit uses a value of K_0=11.0 GPa and K'_0=5.5 and provides now also the initial values of the second-order Grüneisen parameters Γ_i. This includes the inherent volume dependence of the Debye and Einstein temperatures in eq. 19 for the later refinement of the quasiharmonic free energy in the next section.

VI. THE COHERENT THERMODYNAMIC MODEL

For the fundamental function, the total free energy, we now use the form:

$$F(T,V) = E_{zT} + F_{qh}(T,V) + F_{ah}(T,V) \qquad (19)$$

where the ground-state energy E_{zT} depends on the parameters V_0, K_0, K'_0. The quasiharmonic contribution $F_{qh}(T,V)$ includes now the full volume dependence in the Debye

15

and Einstein temperatures as well as in the Grüneisen parameters (8)-(10). The volume dependence in the explicit premelting anharmonicity (16)-(18) is taken into account by the assumption that the characteristic temperature T_a in theses relations is replaced by the volume dependent form:

$$T_{ah}(V) = T_a(V/V_0)^{-\gamma_{ah}} \tag{20}$$

providing the form:

$$F_{ah}(T,V) = F_a(T, T_{ah}(V)) \tag{21}$$

and the volume dependence in other thermodynamic relations (16,18).

The refinement of the 8 weights w_i together with the 8 times three parameters θ_i, γ_i, and Γ_i of the quasi-harmonic model makes use of the fact that there is a certain hierarchy in the dependence of the various thermodynamic functions on these parameters. This means that we can use the preliminary values obtained from the uncorrelated fits as starting values at first for the refinement of the Debye and Einstein temperatures θ_i and the weights w_i in the fit of the heat capacity data, now with the thermodynamically correct forms with the full temperature dependence of all the Debye and Einstein temperatures. In the next step the γ_i are refined with respect to the volume expansion, and in the last step the Γ_i with respect to temperature dependence of the bulk modulus at ambient pressure. With a few cycles of this procedure, we obtain the final values given in Table IV shown in the Appendix.

Small changes in the values of the parameters for the PG-transition were also tested giving the final results for the volume expansion (w_{Vpg} = -2.38·10^{-5}, T_{Vpg} = 122 K, ΔT_{Vpg} = 8.15 K in (C1)) and for the heat capacity (w_{Cpg} = 0.25, T_{Cpg} = 107 K, ΔT_{Cpg} = 22 K in (15)). The available data of the PG-transition observed in the heat capacity did not allow to extract any reasonable information on the volume dependence of this contribution. Since it is difficult to provide an equilibrium thermodynamic relation for the relaxation at lower temperatures[34], theses minor effects would have to be added separately with parameters values depending on the experimental and sample conditions.

The premelting anharmonicity is modeled with the parameters w_a = 7·10^{-5} and T_a= 340 K and the volume dependence of $T_{ah}(V)$ in eq. 20 with the Grüneisen parameter γ_a = -3.5 taken from the melting curve, because this extra "anharmonicity" is closely related to

melting.
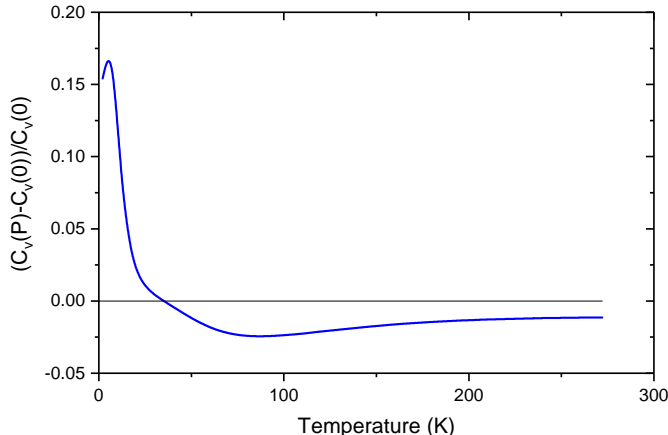
FIG. 8. Relative change of the heat capacity by 2% compression corresponding to the complete range of stability of ice Ih.

VII. PREDICTIVE POWER OF THE PRESENT MODEL

Since the results of the global fit described in the previous chapter do not show any significant difference with respect to the results of the restricted fit to the heat capacity shown in fig. 3, this figure needs no duplication. Similarly, the differences in the fit of the volume expansion were marginal and we find that the additional constraint in the coherent model leads only to a very minor increase of 0.8% in the standard deviations. Without the contribution from the PG-transition the RMSD would increase by 3%. This indicates again that a small contribution from this transition can be noticed also clearly in the volume expansion derived from the neutron diffraction data[6]. The data for the bulk modulus at ambient pressure[6] are also fitted perfectly with no visible difference to the black fitted curve in fig. 7 and provides in this way the values for the refined second-order Grüneisen parameters given in Table IV.

With the coherent thermodynamic model one can now calculate all the thermo-physical properties of ice Ih from the free energy (19) for the whole range of stability form the initial volume $V_0 = 19.30448$ cm^3/mol to the smallest volume $V_{tr} = 18.947$ cm^3/mol, both at 0 K.
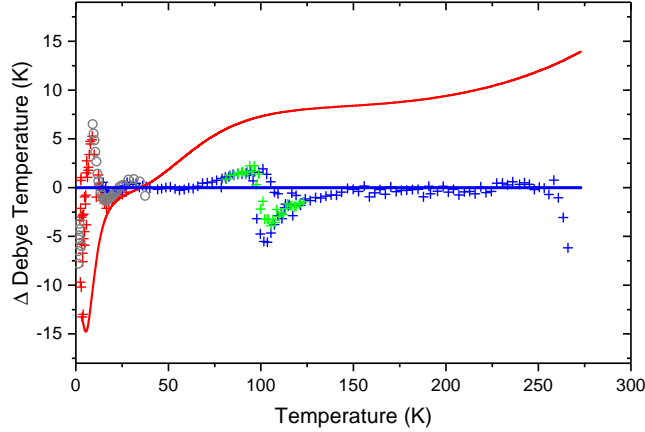
FIG. 9. Effect of pressure on the calorimetric Debye temperature (red curve) with respect to variation at ambient temperature taken as blue base line. In addition, the deviation of the values calculated from the experimental C_v-data for ambient pressure[7,10,11] (symbols) are illustrated for comparison with fig. 4.

Since the effect of pressure on the heat capacity in this small range of compression is rather small, only the relative change is illustrated here in fig. 8.

One can notice here that this relative change becomes rather large only at low temperature due to the large negative values of the Grüneisen parameters for the low-frequency modes. The small maximum around 10 K can be related to the difference of the Grüneisen parameters for this range.

The effect of pressure on the heat capacity may be seen more clearly in fig. 9, which presents the change of the calorimetric Debye temperature by the red curve with respect to the variation at ambient pressure as blue base-line. In addition, fig. 9 shows also the deviation of the values for ambient pressure calculated from the experimental C_v data[7,10,11] with respect to the model curve for comparison with fig. 4, illustrating again the uncertainty below 10 K due to possible effects of disorder and around 100 K due to the PG-transition. The red curve shows quantitatively at low temperatures the predicted decrease due to the negative Grüneisen parameters and at higher temperatures the increase due to the positive values for the higher phonon energies.

In comparison with the small changes of the heat capacity under pressure, the thermal
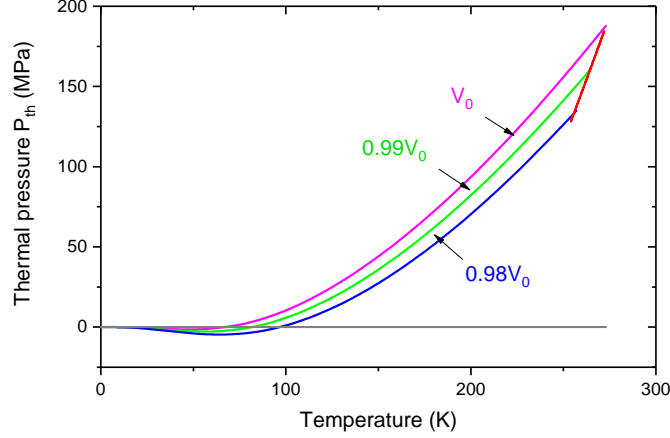
FIG. 10. Isochores for the thermal pressure $P_{th}(V,T)$ at V_0, the volume at ambient pressure and 0 K. The two other values 0.99 V_0 and 0.98 V_0 cover roughly the range of stability of ice Ih (pink, green, blue curves) with the variation along the melting curve (solid red line), corresponding to the free energy (19) with the parameters of Table II. The contribution from the PG-transition is too small to be noticed here.

pressure shows much stronger changes as illustrated in fig. 10.

Isochores for the isothermal bulk modulus for the same range up to the melting curve are presented in fig. 11, which does not show any anomalous behavior.

The equation of states (EOS) can be calculated from (19)

$$P(T,V) = \partial F(T,V)/\partial V = P_{zT} + P_{qh}(T,V) + P_{ah}(T,V) \tag{22}$$

either in the form of isochors or by inversion in the form of isobars $V(T,P)$. Corresponding to the two terms of the thermal contribution to the free energy, the thermal pressure includes also a contribution from the premelting anharmonicity

$$P_{ah}(T,V) = \frac{\gamma_{ah}}{V} U_{ah}(T,V) \tag{23}$$

and one gets for the isobaric volume the implicit form

$$V(T,P) = V_0 \left[1 - \frac{K_0'}{K_0}(P_{th}(T,V(T,P)) - P) \right]^{1/K_0'} - \Delta V_{pg}(T) \tag{24}$$

19
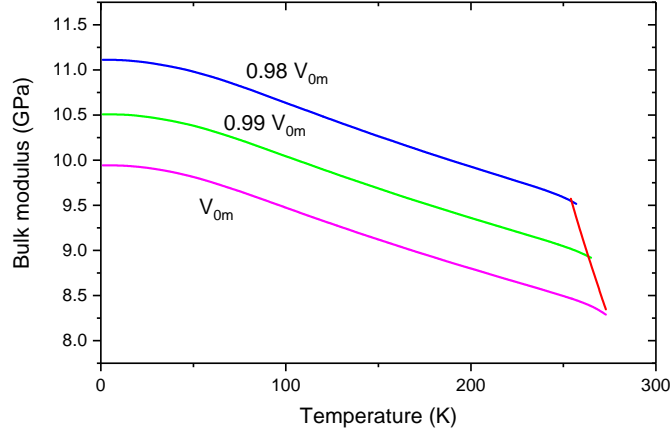
FIG. 11. Isochores for the isothermal bulk modulus $K(V, T)$ at V_{m0}, 0.99 V_{m0} and 0.98 V_{m0} cover roughly the range of stability of ice Ih (pink, green, blue curves) and the variation along the melting curve (red line). V_{m0} is the volume at the melting point at zero pressure.

which can be solved with our reference values K_0=11 GPa and K_0'=6.6 by iteration to get the three isobars for 0, 100 and for 213 MPa covering the range up to the first high pressure phases as shown in fig. 12. Numerical values are given in the appendix V.

One may notice that the negative thermal expansion is barely visible and the effect of the PG-transition can not be seen on this scale in fig. 12. More interesting are therefore the isobars for the thermal expansion coefficient, $\alpha(T, P)$, illustrated in fig. 13.

Here one can notice the similarity to the thermal pressure illustrated in fig. 10, with, however, the region of negative values shifted to smaller temperatures, the expected decrease under compression along the melting curve and larger negative values at low temperatures.

More interesting are the isotherms for the isothermal bulk modulus in fig. 14. The isothermal variations look here almost like straight lines, but the two isobars for ambient pressure and the transition pressure of 213 MPa illustrate the anomalous behavior of ice Ih. On the other hand, the isotherms $P(V, T)$ (fig. 15) for the total pressure show more directly the anomaly of ice Ih by the fact that the 0 K isotherm overlaps with the 50 K isotherm and the 100 K isotherm appears to be shifted downwards.

The present model allows also to calculate the calorimetric Grüneisen parameter:
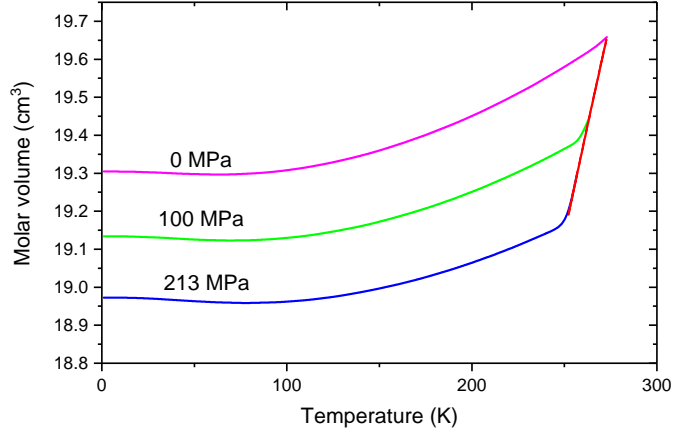
FIG. 12. Isobars for the molar volume $V(T, P)$ for $P=$ 0, 100 and 213 MPa (pink, green, blue curves) and the variation along the melting curve (red line).
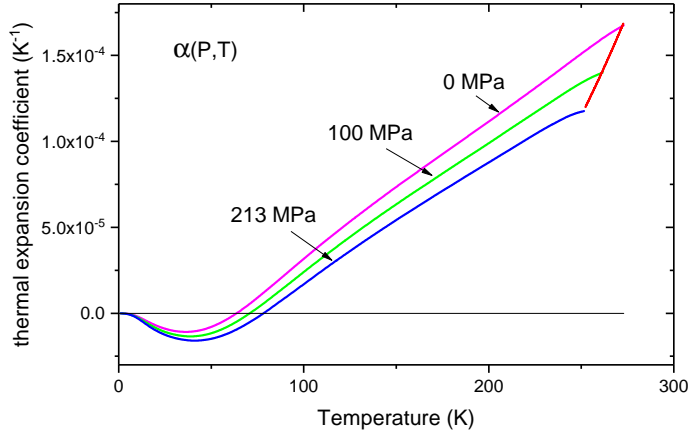
FIG. 13. Isobars for the thermal expansion coefficient $\alpha(T, P)$ for $P = 0$, 100 and 213 MPa (pink, green, blue curves) and the variation along the melting curve (red line).

$$\gamma_{cal}(T, V) = \alpha(T, V) V K(T, V) / C_V(T, V) \tag{25}$$

and its isobaric variation. Two isobars are represented in fig. 16, one for ambient pressure and one for the upper boundary of ice Ih, at 210 MPa.

21
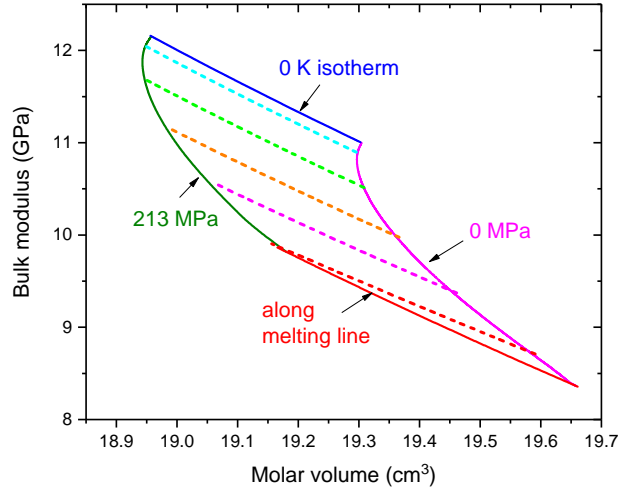
FIG. 14. Isobaric variation of the isothermal bulk modulus at ambient pressure (pink curve) and along the upper boundary of ice Ih at 213 MPa (dark green curve) together with the isotherms for 0 K (blue line), 50 K (turquoise dotted), 100 K (green dotted), 150 K (orange dotted), 200 K (pink dotted), 250 K (red dotted) and along the melting line (red line).

One can notice in fig. 16 a significant effect of pressure on the calorimetric Grüneisen parameter in the temperature range from 10 to about 150 K which is mostly related to the decrease in the corresponding Debye temperature, or, in other words, to negative mode Grüneisen parameters of the low frequency translational modes shown in the next two figs. 17 and 18.

Most remarkable in fig. 17 is the strong decrease of the initial Debye temperature θ_0 and even stronger decrease in the first Einstein temperature θ_1 in the given range of compression and the fact that the decrease becomes even stronger but with finite values at the phase boundary. The increase in θ_4 and θ_5 illustrates that the range of the translational modes is broadening and the almost constant values of θ_6 and θ_7 show that the librational modes are barely effected by this compression. These observation could be compared also with some of the optical studies.

The second-order Grüneisen parameters given in Table IV can be used to calculate also the volume dependencies of the corresponding mode-Grüneisen parameters given in fig. 18. The most significant observation is here again the strong decrease of the initial Debye and the first Einstein term. The intermediate terms 2 to 5 show no systematics and may be effected by

22
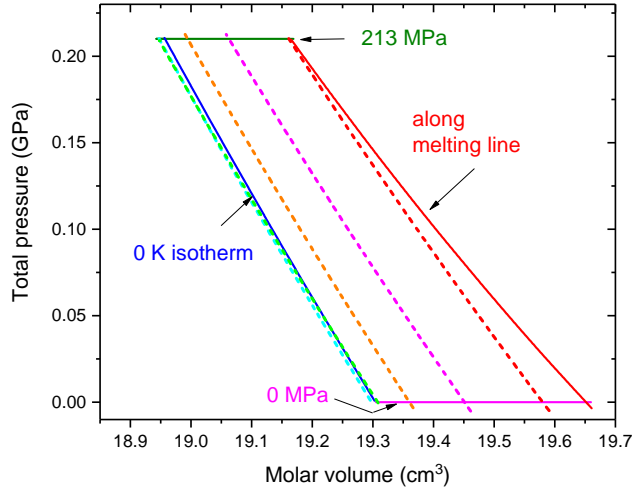
FIG. 15. Isothermal variation of total pressure at 0 K (blue line) and at five temperatures, 50, 100, 150, 200, 250 K (dotted lines) and along the melting curve (red line) up to 213 K. The two isobars for ambient pressure (pink line) and for the transition pressure of 213 MPa frame the isotherms.

contributions from intrinsic anharmonicity not separately modeled in this coherent approach which did not yet take into account the additional information provided by studies on the PDOS to be discussed in the next section.

VIII.   COMPARISON WITH PDOS

When we compare the results of the present model with experimental data for the PDOS of ice Ih[13] from neutron scattering, we can see in fig. 19 that the selected Einstein terms reproduce reasonably well the dominant features of the experimental PDOS.

Since the original data for the PDOS of ice Ih from neutron scattering[13] where not available in numerical form, we digitized the corresponding part of the original fig. 2[13] and scaled the area to 3 modes per molecule, whereby we did not correct for the missing part below 30 K. Integration of this PDOS using the standard formula gave the C_v-data shown in fig. 20 (blue dots). For this purpose, the background of the PDOS was reduced by 3% with respect to the value of the first peak to obtain a better fit of C_v below 100 K.

Fig. 20 (upper) shows at first that in the range below 100 K the heat capacity (red curve) is reproduced very well by values calculated from the experimental PDOS[13] (blue points).
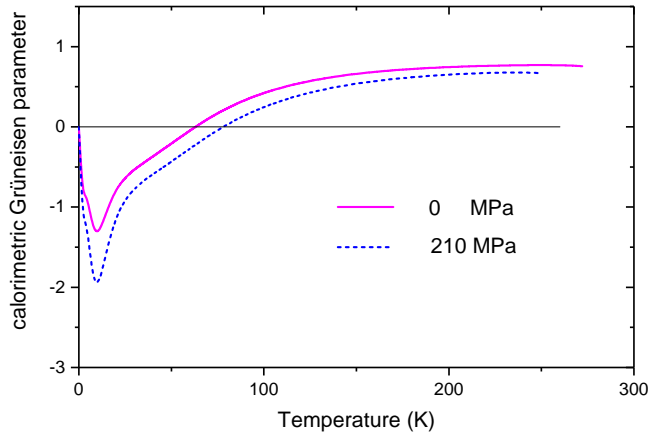
FIG. 16. Comparison of the calorimetric Grüneisen parameter from the present model for ambient pressure (pink curve) and for the upper boundary of ice Ih at 210 MPa (blue dashed curve).
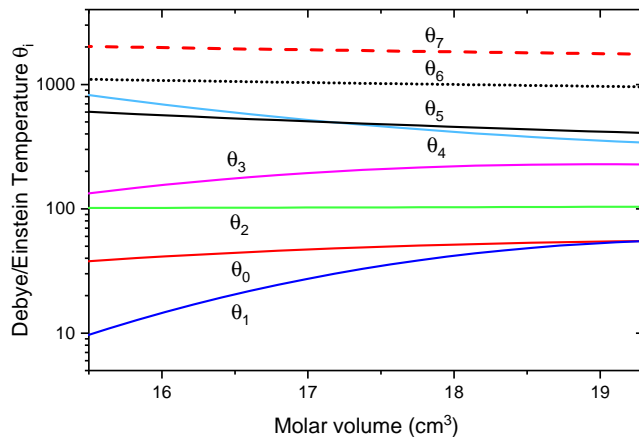
FIG. 17. Volume dependence of the Debye (θ_0) and Einstein (θ_1-θ_7) temperatures.

The comparison with the present coherent model based on formula (19) and using only the first 6 terms (0 to 5 in Table IV) (green dashed line) shows a slight deviation above 100 K which is attributed to anharmonic contributions of these translational modes. An accurate estimate of the anharmonicity of the librational modes could only be made by a detailed comparison with not yet available data for the librational PDOS. However, for the

24
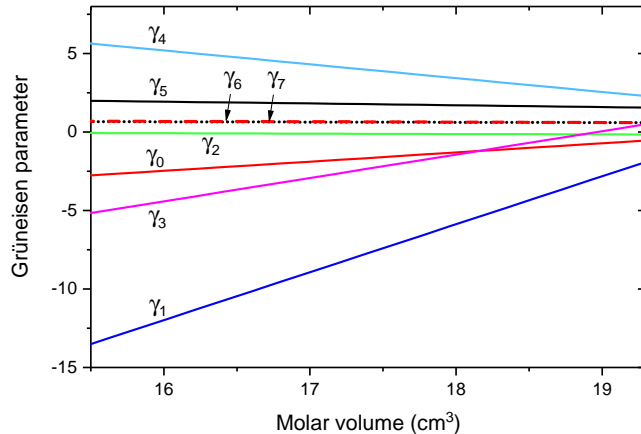
FIG. 18. Volume dependence of the Grüneisen parameters for the Debye (θ_0) and Einstein (θ_1-θ_7) temperatures of the present model.

translational modes we get within our model a total weight of 3.188 in comparison with the expected 3 per molecule. We attribute this 6% deviation to explicite anharmonicity and model it - in a first approach - within our quasi-harmonic approximation simply by the excess weights of the θ_0-θ_5 terms.

It is then not clear how to distribute this anharmonicity over the six terms representing the translational modes. If we use an equal distribution over the 6 terms we get a large deviation at low temperatures with respect to the values calculated from the PDOS as shown in fig. 20 (lower) by the green curve. On the other hand, when the anharmonicity is completely attributed to the highest translational term, θ_5, we get the pink curve with small deviations to lower values in the higher temperature range. The best compromise is apparently obtained by equal distribution over both the LO and TO translational modes, θ_4 and θ_5. The corresponding orange line in fig. 20 (lower) shows now some deviations below 50 K which can be attributed to the cutoff and background correction in the PDOS.

At this point we can also compare the theoretical PDOS[15] with the experimental data for the heat capacity, as shown in fig. 20 as grey curve. The theoretical PDOS was extracted from a lattice dynamical model based on neutron scattering measurements of the low-energy phonon dispersion curves up to 19 meV corresponding to 220 K. Fig. 21 compares the experimental PDOS[13] with the theoretical PDOS[15] and earlier data of the neutron scattering
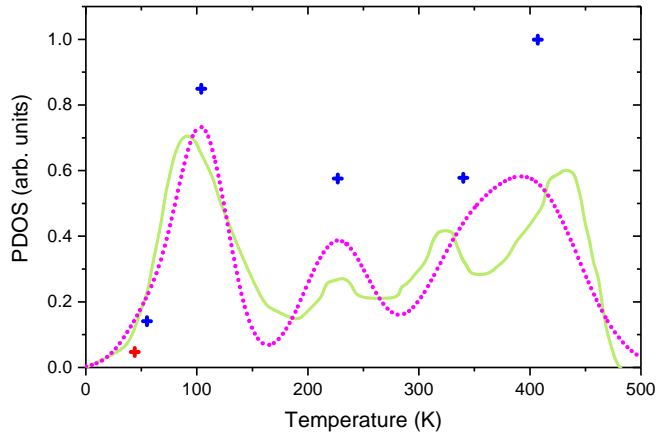
FIG. 19. PDOS for the translational modes of ice Ih from neutron scattering[13] (green curve) compared with dominant features of the present model, whereby the red cross represents the weight of the Debye term, the blue crosses mark the Einstein terms and the pink curve corresponds to a broadening of the Einstein terms by Gaussians of suitable width.

TABLE III. Parameters for the "constrained" quasi-harmonic model with implicite anharmonicity.

	0	1	2	3	4	5	6	7
$\theta_i(K)$	55	55	104	227	340	407	830	1160
w_i	0.044	0.141	0.849	0.576	0.578	0.813	0.300	2.700
β_i	0.0	0.0	0.03	1.14	0.17	0.28	23.00	3.40

function[14]. It provides some additional information on the PDOS since it represent its typical features but not the correct relative intensities.

One can see clearly in fig. 21 that the high energy part of the theoretical PDOS[15] shows a too small TO-LO-splitting and a total shift to lower energies in comparison with the corresponding structures in both the experimental PDOS[13] and the scattering function[14]. In the low energy part a significant shift is most clearly visible around 150 K. Theses differences illustrate that the lattice dynamical model[12,15] helps very much in understanding the structure of the PDOS, but does not yet provide accurate data for the description of a thermodynamical model covering the whole energy range. In fact this point had already been
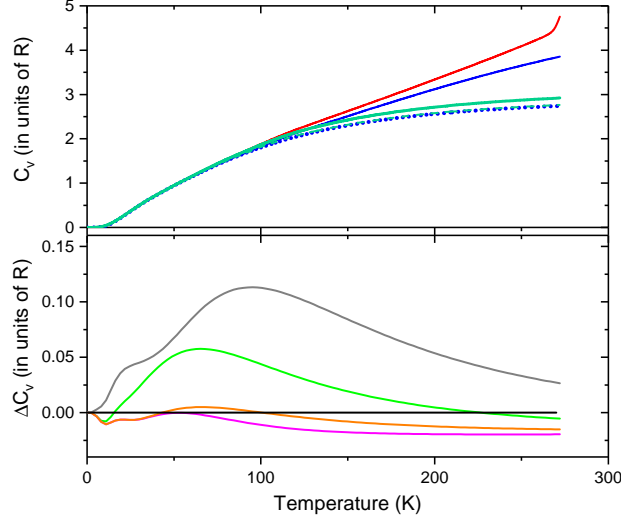
FIG. 20. Upper: Heat capacity of ice Ih at ambient pressure (red line) compared with values calculated from the experimental PDOS[13] (blue dots) including only the translational modes as shown in fig. 19 and from the present coherent model (green dashed line) using only the first 6 terms (0-5). An estimate of the anharmonicity in the translational modes results in the green solid line and the blue line illustrates the total harmonic contribution including the librational modes. Lower: Difference between the quasi-harmonic heat capacity obtained by the experimental PDOS[13] (dotted blue line in the upper plot) and values obtained with different distributions of the translational anharmonicity. The green curve corresponds to an equal distribution over all the translational terms (θ_0 to θ_5), the pink curve to anharmonicity only on the θ_5 term, and the orange curve to an equal distribution over θ_4 and θ_5. The gray curve represents the surplus of the heat capacity calculated from the theoretical PDOS[15].

indicated by the author of the model[12]. Also, the more recent theoretical models[17,19] provide primarily a better understanding of the physical background, and the comparison of their results with the experimental data serves as a guide for the choice of the best approximations to be used in theses models.

So far we have compared our results only with the PDOS data for the translational modes (below 500 K, see fig. 22). For higher energies (fig. 22) only the neutron scattering function is available which cannot be converted easily into a PDOS but provides at least the positions of its characteristic features described by the θ_6 and θ_7 terms of the present model.

Since we expect in the strictly harmonic approximation for the librational modes a total
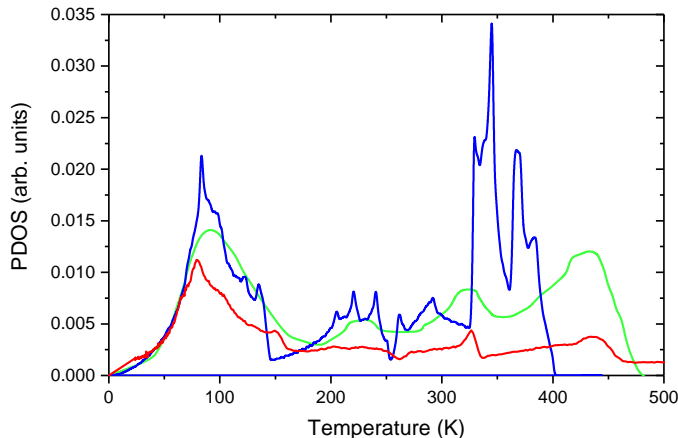
FIG. 21. Comparison of the experimental PDOS[13] (green curve) with the theoretical PDOS[15] (blue curve) and the neutron scattering function[14] (red curve with roughly adjusted scale).

weight of 3 per molecule, we see that this value is nearly reached already by the θ_6 term, and the large weight of the θ_7 term must be attributed mostly to anharmonic contributions.

So far we have used what we call a quasi-harmonic approximation which models the anharmonicity just by excess weights of the quasi-harmonic terms. In this way we have limited the number of free parameters of the present approach. However, more correctly we should have used a quasi-harmonic approach with the correctly constrained weights (or number of modes per molecule) together with an implicit anharmonic contribution for each mode. This implicit anharmonicity is commonly related to a temperature dependence of the quasi-harmonic frequencies at constant volume[8,28,29,47] and can be approximated in first order by an anharmonic contribution proportional to the internal energy of the mode i, scaled by a factor β_i, i.e. $(1 + \beta_i u_i(T, \theta_i)/(k_B \theta_i))$. When we applied this scheme to the representation of the heat capacity, we noticed first of all that the θ_7 term had to be shifted into the region of the librational modes together with a smaller shift of the θ_6 term and a dramatic change in the weights of these two terms as indicated by the values given in Table III with the new harmonic weights w_i and the additional anharmonicity parameters β_i.

One may notice also in Table III that we need no anharmonic contribution for the first two terms and have to change for the translational modes only the weight of the highest

28
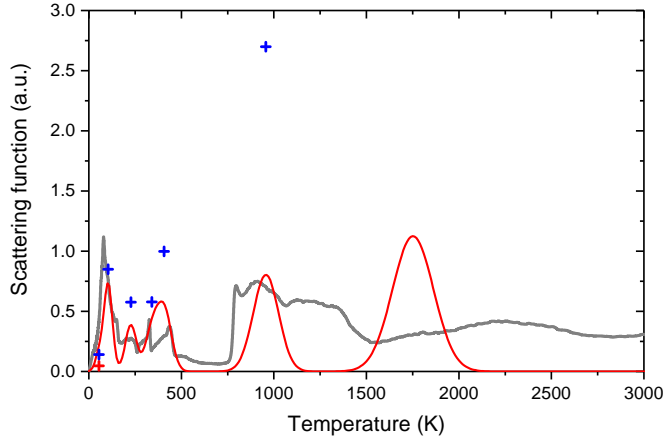
FIG. 22. Comparison of the neutron scattering function[14] (gray curve) with Debye and the Einstein terms of the present model (red and blue crosses represent weights). The weight $w_7 = 6.25$ is out of scale and only represented by the area of the corresponding Gaussian at $\theta_7 = 1752$ K together with Gaussians for the other terms (red curve).

term θ_5. Since the anharmonicity parameters of the librational modes are strongly correlated with the values of the representative frequencies, we did not attempt to refine the parameters perfectly. In fact, the representative Einstein terms should be determined with respect to a reliable PDOS, which is not yet available. Any extra volume dependence of the anharmonicity parameters has been neglected here and could be handled by an increase in the number of free parameters which could not be constrained by any experimental data at the present time. From this point of view fig. 23 shows now only that this quasi-harmonic approach with the parameters of Table IV fits the experimental data for the specific heat almost as good as the refined unconstrained model. But the distribution of the anharmonicity is physically more reasonable in this constrained approach and allows therefore also for a better estimate of the remaining (systematic) uncertainties.

In any case we can notice that the anharmonic contributions to the translational modes are very moderate and their pressure dependence does not introduce significant uncertainties in any of the thermodynamic relations at moderate temperatures (T < 100). The effect of pressure on the anharmonicity of the librational modes could be positive or negative, and even as a small contribution it represents now the larges uncertainty in the prediction of
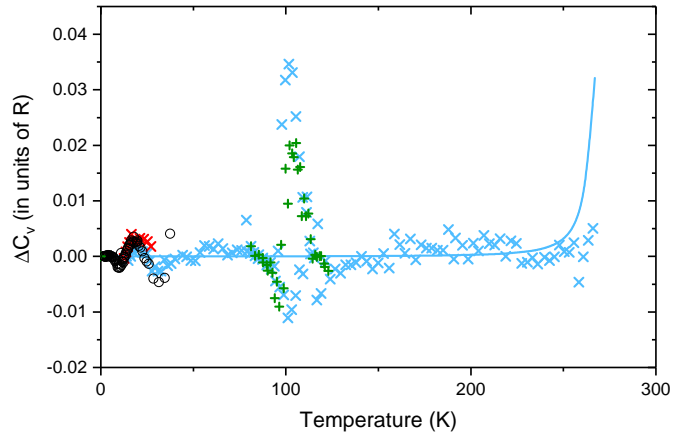
FIG. 23. Deviations of the experimental data for the heat capacity from the representation by the "constrained" quasi-harmonic model with explicit anharmonic contributions. The contribution from the PG-transition has been subtracted like in fig. 3 together with the extra premelting anharmonicity, which is indicated here by the light blue line.

the behavior of ice Ih under pressure. However, studies of the anharmonicity of ice Ih single crystals by X-ray diffraction[33] indicate that there could be a chance to constrain this uncertainty by an extension of this type of studies in the future also to high pressures.

IX. GRÜNEISEN PARAMETERS

So far we have not yet compared the present results with the study of the effect of pressure on the dispersion of the Grüneisen parameters under compression[15]. Although the phonon dispersion curves under pressure were studies by neutron scattering, a lattice dynamical model was needed to extract the dispersion of the Grüneisen parameters for some high symmetry directions in reciprocal space[15]. One of the most prominent observations concerns the large negative values (approximately -2.7) of the mode Grüneisen parameters along the Γ-M-direction. However, the energy dependent average over all the directions in reciprocal space needed for a comparison with the present results was not given and could not be generated easily from the graphical representation of the dispersion curves. Nevertheless the presentation of the PDOS for 0.05 and 0.5 GPa (provided in digital form by the authors)
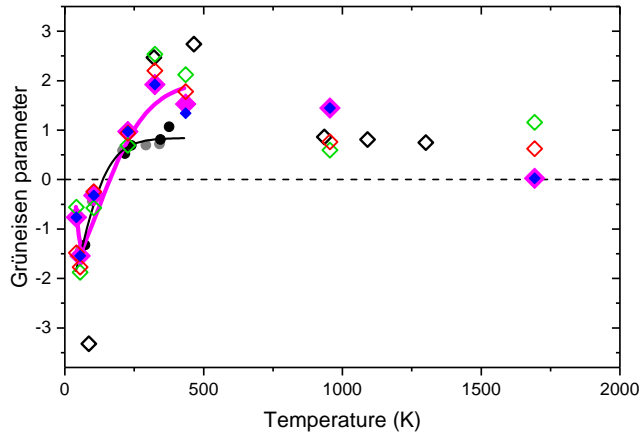
FIG. 24. Energy dependence of the Grüneisen parameters in terms of Einstein temperatures. Reciprocal space-averaged mode Grüneisen parameters from a lattice dynamical model[15] (gray and black points with black curve as guide to the eye) and data from a computer simulation[17] (black open diamonds), values from the present model (row 6 in Table II) based on the reference data for the bulk modulus (pink diamond with pink connecting line). The other data from Table II, are shown as small green, red, and blue open diamonds respectively, to illustrate the uncertainty related to the different literature data for the thermal expansion[4–6].

allowed us to extract a few values for this energy dependent average Grüneisen parameter from the shifts of some prominent features in theses spectra, which are presented in fig. 24.

At first one may notice reasonably good agreement between the lattice dynamical data[15] and the present data at low energies (below 100 K) and than significantly smaller absolute values with respect to the computer simulation[17]. The values for the librational modes with phonon energies between 800 to 1700 K are obviously not well constrained by the present model due to the influence of effects from anharmonicity and lattice defects.

X. DISCUSSION

Although ice Ih appears at first to be a simple molecular crystal, it shows a very complex behavior which is not yet completely understood. It is clear that the phonon spectrum is separated into 4 distinct regions with the translational modes at the lowest energy (up to

400 K in temperature units), the librational modes from about 700 to 1500 K, the bending modes from 2300 to 2600 K and the stretching modes around 4900 K. However, good values for the corresponding PDOS are only available for the translational modes which leads to the problem that the anharmonic contributions to the thermodynamic properties are well constrained only in the low temperature region (< 150 K) and their unknown pressure dependence limits the accuracy of the present modeling at higher temperatures and elevated pressures. At very low temperatures (< 10 K) possible effects from a quantum glass behavior limit the accuracy of the present thermodynamic model. Furthermore, the lack of a good model for the "proton glass transition" does not yet allow an accurate formulation of the entropy. This effects also the evaluation of the thermal expansion and the related Grüneisen parameters, especially due to the fact, that the small but significant difference between the microscopic and macroscopic determinations of the volume expansion is not yet well understood. Nevertheless, the evaluation of all the experimental data for the present thermodynamic model can be considered as a good basis for the selection of the best approximations to be used in theoretical models which have provided so far a better understanding of the physical phenomena relevant for ice Ih, but still with limited accuracy as far as a comparison with experimental data is concerned. Cold ice remains a hot topic!

ACKNOWLEDGMENTS

Appendix A: Thermodynamic relations

For one Einstein term, the form of the internal energy, heat capacity, thermal pressure and isothermal bulk modulus are given by:

$$u_E(T, \theta) = \frac{k_B \theta}{exp(\theta/T) - 1} \tag{A1}$$

$$c_E(T, \theta) = k_B \left[\frac{2T}{\theta} sinh(\frac{\theta}{2T}) \right]^{-2} \tag{A2}$$

$$p_E(T, \theta, \gamma) = \frac{\gamma}{V} u_E(T, \theta) \tag{A3}$$

$$k_E(T, \theta, \gamma, \Gamma) = (1 + \gamma_E - \Gamma_E) \cdot p_E(T, \theta) - \frac{\gamma_E^2 T}{V} c_E(T, \theta) \tag{A4}$$

For one Debye term, the free energy $f_D(T, \theta_D)$, internal energy $u_D(T, \theta)$, heat capacity $c_D(T, \theta)$, are given by:

$$f_D(T, \theta_D) = 3k_B\theta_D \left(\frac{T}{\theta_D}\right)^4 \int_0^{\theta_D/T} x^2 ln(1 - exp(-x)) dx \tag{A5}$$

$$u_D(T, \theta_D) = 3k_B\theta_D \left(\frac{T}{\theta_D}\right)^4 \int_0^{\theta_D/T} \frac{x^3}{exp(x) - 1} dx \tag{A6}$$

$$c_D(T, \theta_D) = \frac{3}{4} k_B \left(\frac{T}{\theta_D}\right)^3 \int_0^{\theta_D/T} \left[\frac{x^2}{sinh(x/2)}\right]^2 dx \tag{A7}$$

The formula for the thermal pressure $p_D(T, \theta, \gamma)$ and thermal contribution to the bulk modulus $k_D(T, \theta, \gamma, \Gamma)$ correspond to the forms (A3) and (A4) with E replaced by D.

Appendix B: Pseudo-Debye forms

The free energy of the pseudo-Debye form consists of a leading term f_{PD_0} for low temperatures:

$$f_{PD_0}(T, \theta) = -k_B(T/3) ln(1 + (\theta/T)^3) \tag{B1}$$

and two Einstein terms f_E in the form of:

$$f_{PD}(T) = w_0 f_{PD_0}(T, \theta) + w_1 f_E(T, f_1\theta) + w_2 f_E(T, f_2\theta) \tag{B2}$$

with the weights w_0=0.05652, w_1=0.90748, w_2=0.036 and the scaling factors f_1=0.81 and f_2=0.41 for the effective (fixed) Einstein temperatures. Since all the other thermodynamic relations for the pseudo-Debye terms are similar sums, only the expressions involving the leading term f_{PD_0} are shown here for the internal energy:

$$u_{PD_0}(T, \theta) = k_B T/(1 + (\theta/T)^3) \tag{B3}$$

and for the heat capacity:

$$c_{PD_0}(T, \theta) = k_B (1 + 4(\theta/T)^3)/(1 + (\theta/T)^3)^2 \tag{B4}$$

which shows that these terms have the same asymptotic behavior at low and high temperatures as the normal Debye form.

Appendix C: Modelling the "proton glass transition"

When we subtract the contribution of the PG-transition in the volume expansion, we use a Gaussian form:

$$\Delta V_{pg}(T) = -V_0 w_{Vpg} exp(-\frac{T - T_{Vpg}}{\Delta T_{Vpg}})^2 \tag{C1}$$

with the weight $w_{Vpg} = 0.00014$, the position $T_{Vpg} = 103$ K and the width $\Delta T_{Vpg} = 14$ K in the fits of the diffraction data which reduces the standard deviation of these by 6%. But with all the uncertainty related to this sluggish feature, we keep this term as a small correction in the thermal expansion and not as a normal contribution to the equilibrium thermodynamics.

For any application of the present model we give here all the parameters of the final refinement in Table IV.

TABLE IV. Values for the parameters of the present 1PD7E-model.

	0	1	2	3	4	5	6	7
$\theta_i(K)$	55	55	104	227	340	407	957	1752
w_i	0.044	0.14	0.851	0.579	0.52	1.068	2.728	5.92
γ_i	-0.914	-1.93	-0.114	0.504	2.282	1.569	0.61	0.61
Γ_i	-22.29	-26.52	1.46	62.51	-6.25	-3.87	0.76	0.66

Appendix D: Calculated specific heat and relative volume change under pressure

DATA AVAILABILITY

TABLE V. Calculated values of the specific heat C_V at ambient pressure (in units of R) and the relative volume change $\Delta V/V_0$ at ambient pressure, 100 MPa and 213 MPa, with 0 K molar volumes of V_0=19.30441 cm^3/mole, 19.13392 cm^3/mole, and 18.97276 cm^3/mole, respectively.

| $T(K)$ | C_V/R | $\Delta V/V_0 \cdot 10^4$ | $\Delta V/V_0 \cdot 10^4$ | $\Delta V/V_0 \cdot 10^4$ |
	0 MPa	0 MPa	100 MPa	213 MPa
0	0	0	0	0
5	0.0030	-0.0013	-0.0015	-0.0018
10	0.0354	-0.0391	-0.0486	-0.0588
15	0.1174	-0.2065	-0.2528	-0.2991
20	0.2393	-0.5198	-0.6268	-0.7302
25	0.3732	-0.9463	-1.1300	-1.3033
30	0.5018	-1.4486	-1.7224	-1.9763
35	0.6216	-1.9903	-2.3696	-2.7166
40	0.7341	-2.5348	-3.0389	-3.4952
45	0.8420	-3.0441	-3.6962	-4.2819
50	0.9471	-3.4803	-4.3066	-5.0445
55	1.0503	-3.8072	-4.8353	-5.7498
60	1.1519	-3.9925	-5.2501	-6.3663
65	1.2520	-4.0088	-5.5230	-6.8652
70	1.3501	-3.8342	-5.6308	-7.2223
75	1.4460	-3.4526	-5.5555	-7.4182
80	1.5394	-2.8525	-5.2839	-7.4382
85	1.6300	-2.0270	-4.8073	-7.2717
90	1.7179	-0.9722	-4.1202	-6.9117
95	1.8031	0.3128	-3.2200	-6.3542
100	1.8858	1.8273	-2.1062	-5.5973
105	1.9661	3.5692	-0.7798	-4.6411
110	2.0443	5.5355	0.7573	-3.4867
115	2.1207	7.7228	2.5023	-2.136
120	2.1955	10.1274	4.4521	-0.5910
125	2.2691	12.7459	6.6037	1.1450
130	2.3415	15.5748	8.9539	3.0693
135	2.4132	18.6107	11.4996	5.1793
140	2.4842	21.8508	14.2379	7.4721
145	2.5548	24.5882	17.1664	9.9452
150	2.6251	28.9338	20.2826	12.5963
155	2.6952	32.7727	23.5847	15.4234
160	2.7654	36.8076	27.0709	18.4246
165	2.8356	41.0376	30.7399	21.5983
170	2.9060	45.4620	34.5905	24.9431
175	2.9767	50.0803	38.6220	28.4581
180	3.0477	54.8925	42.8339	32.1423
185	3.1190	59.8988	47.2260	35.9950
190	3.1908	65.0998	51.7982	40.0159
195	3.2630	70.4964	56.5508	44.2045
200	3.3357	76.0897	61.4842	48.5608
205	3.4089	81.8810	66.5991	53.0845
210	3.4826	87.8718	71.8960	57.7756
215	3.5568	94.0640	77.3757	62.6336
220	3.6316	100.4594	83.0390	67.6581
225	3.7068	107.0599	88.8865	72.8477
230	3.7825	113.8677	94.9185	78.2002
235	3.8588	120.8845	101.1347	83.7113
240	3.9356	21.8508	107.5337	89.3735
245	4.0131	135.5518	114.1124	95.1724
250	4.0915	143.2040	120.8647	101.0797
255	4.1713	151.0679	127.7783	148.9460
260	4.2544	159.1405	134.8293	209.0238
265	4.3482	167.4146	181.8177	268.3027

Additional data of this study are available from the corresponding author upon request.

REFERENCES

[1] P. Bridgman, "Water, in the liquid and five solid forms, under pressure," Proc. Am. Acad. Arts Sci. **47**, 441 (2012).

[2] R. Feistel and W. Wagner, "A new equation of state for H_2O ice Ih," J. Phys. Chem. Ref. Data **35**, 1021 (2006).

[3] M. Choukroun and O. Grasset, "Thermodynamic model for water and high-pressure ices up to 2.2 GPa and down to the metastable domain," J. Chem. Phys. **127**, 124506 (2007).

[4] K. Röttger, A. Endriss, J. Ihringer, S. Doyle, and W. Kuhs, "Lattice constants and thermal expansion of H_2O and D_2O ice Ih between 10 and 265 K," Acta Cryst. Sect. B **50**, 644 (1994).

[5] D. Buckingham, J. Neumeier, S. Masunaga, and Y. Yi-Kuo, "Thermal expansion of single-crystal H_2O and D_2O ice Ih," Phys. Rev. Lett. **121**, 185505 (2018).

[6] A. Fortes, "Accurate and precise lattice parameters of H_2O and D_2O ice Ih between 1.6 and 270 K from high-resolution time-of-flight neutron powder diffraction," Acta Crys. B. **74**, 196 (2018).

[7] A. Flubacher, A. Leadbetter, and J. Morrison, "Heat Capacity of Ice at Low Temperatures," J. Chem. Phys. **33**, 1751 (1960).

[8] A. Leadbetter, "The thermodynamic and vibrational properties of H_2O and D_2O," Proc. Royal Soc. A **287**, 403 (1965).

[9] M. Sugisaki, H. Suga, and S. Seki, "Calorimetric study of the glassy state. iv. heat capacities of glassy water and cubic ice," Bull. Chem. Soc. Japan **41**, 2591 (1968).

[10] O. Haida, T. Matsuo, H. Suga, and S. Seki, "Calorimetric study of the glassy state X. Enthalpy relaxation at the glass-transition temperature of hexagonal ice," J. Chem. Thermodyn. **6**, 815 (1974).

[11] S. Smith, B. Lang, S. Liu, J. Boerio-Goates, and B. Woodfield, "Heat capacities and thermodynamic functions of hexagonal ice from T = 0.5 K to T = 38 K," J. Chem. Thermodyn. **39**, 712 (2007).

[12] B. Renker, "Lattice dynamics of hexagonal ice," *Physics and Chemistry of Ice*, eds. E. Walley, S.J. Jones; and L.W. Gold, Royal Society of Canada, Ottawa (1973).

[13]D. Klug, E. Whalley, E. Svensson, J. Root, and V. Sears, "Densities of vibrational states and heat capacities of crystalline and amorphous H_2O ice determined by neutron scattering," Phys. Rev. B **44**, 841 (1991).

[14]J.-C. Li, "Inelastic neutron scattering studies of hydrogen bonding in ices," J. Chem. Phys. **105**, 6733 (1996).

[15]T. Strässle, A. Saitta, S. Klotz, and M. Braden, "Phonon dispersion of ice under pressure," Phys. Rev. Lett **93**, 225901 (2004).

[16]J.-L. Kuo, M. Klein, and W. Kuhs, "The effect of proton disorder on the structure of ice-Ih: A theoretical study," J. Chem. Phys. **123**, 124505 (2005).

[17]R. Ramirez, N. Neuenburg, M. Fernandez-Serra, and C. Herro, "Quasi-harmonic approximation of thermodynamic properties of ice Ih,II, and III," J. Chem. Phys. **137**, 044502 (2012).

[18]O. Benton, O. Sikora, and N. Shannon, "Classical and quantum theories of proton disorder in hexagonal water ice," Phys. Rev. B **93**, 125143 (2016).

[19]M. Salim, S. Willow, and S. Hirata, "Ice Ih anomalies: Thermal contraction, anomalous volume isotope effect, and pressureinduced amorphization," J. Chem. Phys. **144**, 204503 (2016).

[20]S. Jackson, V. Nield, R. Whithworth, M. Oguro, and C. Wilson, "Single cryst. Neutron Struc. Ice XI," J. Phys. Chem. B **101**, 6142 (1997).

[21]A. Fortes, "Structural manifestation of partial proton ordering and defect mobility in ice Ih," Phys. Chem. Chem. Phys **21**, 8264 (2019).

[22]K. Huang, "Statistical Mechanics," *Statistical Mechanics*, J. Wiley & and Sons, New York (1963).

[23]G. Falk, "Physik - Zahl und Realität," Birkhäuser Verlag, Basel (1990).

[24]F. Murnaghan, "Finite deformations of an elastic solid," Am. J. Math. **59**, 235 (1937).

[25]P. Debye, "Zur Theorie der spezifischen Wärmen," Ann. Phys. **39**, 789 (1912).

[26]W. Holzapfel, "Approximate EOS for solids from limited data sets," J. Phys. Chem. Solids **55**, 711 (1994).

[27]W. Holzapfel, "EOS for solids under strong compression," High Press. Res. **16**, 81–126 (1998).

[28]W. Holzapfel, "Equations of state for rare gas solids under strong compression," J. Low. Temp. Phys. **122**, 401–412 (2001).

[29] W. Holzapfel, M. Hartwig, and W. Sievers, "Equations of state for Cu, Ag, and Au for wide ranges in temperature and pressure up to 500 GPa and above," J. Phys. Chem. Ref. Data. **30**, 515–529 (2001).

[30] L. Pauling, "The structure and entropy of ice and of other crystals with some randomness of atomic arrangement," J. Am. Chem. Soc. **57**, 2680 (1935).

[31] W. Kuhs and M. Lehmann, in: *Water Science Review* vol. 1, ed. F. Franks, Cambridge Univ. Press, Cambridge (1986).

[32] W. Kuhs and M. Lehmann, "The geometry and orientation of the water moleculein ice Ih," J. de Phys. Colloq. (Paris) **48 (C1)**, 3–8 (1987).

[33] A. Goto, T. Hondoh, and S. Mae, "The electron density distribution in ice ih determined by single-crystal x-ray diffractometry," J. Chem. Phys. **93**, 1412 (1990).

[34] M. Tyagi and S. Murthy, "Dielectric relaxation in ice and ice clathrates and its connection to the low-temperature phase transition induced by alkali hydroxides as dopants," J. Phys. Chem. **A 106**, 5072–5080 (2002).

[35] A. Karasevskii and W. Holzapfel, "Influence of vibrational anharmonicity and vacancies on thermodynamic properties of the rare gas crystals," Fizika Nizkikh Temp. **29**, 951–956 (2003).

[36] A. Karasevskii, W. Holzapfel, and V. Lubashenko, "Vacancies structure of crystals at high temperature. thermodynamic properties and melting," J. Low. Temp. Phys. **139**, 609 (2005).

[37] R. Pynn, "The 0 K Debye temperature of hexagonal-close packed materials," Can. J. Phys. **49**, 1690 (1971).

[38] J. Poirier, "Introduction to the Physics of the Earth's Interior," *Introduction to the Physics of the Earth's Interior*, Cambridge Unviversity Press, Cambridge (1974).

[39] S. Hunklinger, "Quantenphänomene in Gläsern," Phys. Blätter **55**, 57 (1999).

[40] R. Gagnon, H. Kiefte, M. Clouter, and E. Whalley, "Pressure dependence of the elastic constants of ice Ih to 2.8 kbar by Brillouin spectroscopy," J. Chem. Phys. **89**, 4522 (1988).

[41] R. Gagnon, H. Kiefte, M. Clouter, and E. Whalley, "Acoustic velocities and densities of polycrystalline ice Ih, II, II, V, and VI by Brillouin spectroscopy," J. Chem. Phys. **92**, 1909 (1990).

[42] T. J. Proctor, "Low-temperature speed of sound in single crystal ice," J. Ac. Soc. Am.. **39**, 972 (1966).

[43] J. Neumeier, "Elastic constants, bulk modulus, and compressibility of H_2O ice Ih for the temperature range 50 K - 273 K," J. Phys. Chem. Ref. Data **47**, 03301 (2018).

[44] P. Gammon, H. Kiefte, and M. Clouter, "Elastic constants of ice samples by Brillouin spectroscopy," J. Phys. Chem. **87**, 4025 (1983).

[45] G. Shaw, "Elastic properties and equation of state of high pressure ice," J. Phys. Chem. **84**, 5862 (1986).

[46] R. Gagnon, H. Kiefte, M. Clouter, and E. Whalley, "Elastic constants of ice Ih, up to 2.8 kbar, by Brillouin spectroscopy," J. Phys. Colloques (C1) **48**, 23 (1987).

[47] D. Wallace, *Thermodynamics of Crystals*, Wiley, New York (1972).